

Learning Fast Monomial Orders for Gröbner Basis Computations

R. Caleb Bunch¹, Alperen A. Ergür², Melika Golestani², Jessie Tong³,
 Malia Walewski⁴, and Yunus E. Zeytuncu⁵

¹Georgia Institute of Technology

²The University of Texas at San Antonio

³San Diego State University

⁴Emory University

⁵University of Michigan–Dearborn

Abstract

The efficiency of Gröbner basis computation, the standard engine for solving systems of polynomial equations, depends on the choice of monomial ordering. Despite a near-continuum of possible monomial orders, most implementations rely on static heuristics such as GrevLex, guided primarily by expert intuition. We address this gap by casting the selection of monomial orderings as a reinforcement learning problem over the space of admissible orderings. Our approach leverages domain-informed reward signals that accurately reflect the computational cost of Gröbner basis computations and admits efficient Monte Carlo estimation. Experiments on benchmark problems from systems biology and computer vision show that the resulting learned policies consistently outperform standard heuristics, yielding substantial reductions in computational cost. Moreover, we find that these policies resist distillation into simple interpretable models, providing empirical evidence that deep reinforcement learning allows the agents to exploit non-linear geometric structure beyond the scope of traditional heuristics.

1 Introduction

Systems of non-linear algebraic equations arise naturally in kinematics [41, 52, 46], cryptography [8, 3, 43], systems biology [45, 21, 15], multiple view geometry [27, 42, 1], statistical inference [14, 51, 2], and discrete optimization [12, 6, 7]. To transform this descriptive power into prescriptive capacity, one must either solve the underlying system of polynomial equations or gain insight on their structure. This is where the challenge lies. Quantifying the intrinsic difficulty of computing the common zeros of polynomial systems precisely is an important ongoing discussion in post-quantum cryptography and complexity theory. We also note that for certain structured problems, alternatives to Gröbner bases may exist. For example, [35] shows that in specific computer vision settings, non-Gröbner bases can lead to faster

minimal solvers. Notwithstanding these discussions, we focus on the most general-purpose and widely applicable method for solving polynomial systems: Gröbner basis computation.

A Gröbner basis can be viewed as a far-reaching generalization of Euclid’s algorithm, extending it from the world of integers to the realm of multivariate polynomial systems and discrete geometry. Remarkably, this extension was formalized more than two millennia after Euclid, with the introduction of Gröbner bases in Buchberger’s thesis [5]. Buchberger also proposed an algorithm for computing such bases, and despite substantial advances over the intervening decades, state-of-the-art methods remain largely refinements of this original framework [17, 18]. These methods are best understood not as fully specified algorithms, but as algorithmic schemes that require the user to make several critical choices. While these choices do not affect theoretical correctness, they can have a dramatic impact on practical computational performance.

To instantiate a Buchberger-style algorithm, two principal decisions must be made: the choice of a monomial ordering and the strategy for selecting pairs for reduction. We carefully define these two notions in the next section. In practice, most implementations default to a small set of standard monomial orderings, such as Lex, GrLex, and GrevLex, despite the existence of a near-continuum of valid alternatives. More precisely, the space of all admissible monomial orderings is encoded by a rich geometric object known as the Gröbner fan. The structure of this fan is largely ignored in current implementations, which instead rely on a handful of default choices derived from expert intuition. In this work, we challenge this convention by casting the selection of monomial orderings as a reinforcement learning problem.

1.1 Our contributions

Our primary contribution demonstrates the potential of reinforcement learning (RL) as a tool for computational algebra by directly challenging the conventional wisdom that GrevLex should serve as the default monomial ordering. Across polynomial systems arising in systems biology and computer vision, our trained agents consistently outperform standard default choices, achieving reductions in computational cost of up to 70% under a rigorously calibrated proxy.

We focus our training and data generation on zero-dimensional polynomial systems, that is, systems with finitely many common solutions. This choice is strategic. For such systems, computing a Gröbner basis with a fast, agent-selected ordering enables efficient conversion to the lexicographical (Lex) ordering using the FGLM algorithm and its modern variants. This capability is essential in applications requiring variable elimination, where direct computation in Lex order is often infeasible. Moreover, across diverse applications of Gröbner basis in sciences and engineering zero-dimensional systems are the ones that appear most of time. This motivates our focus on zero dimensional ideals.

We design a reinforcement learning environment in which agents learn to select optimized monomial orderings. To the best of our knowledge, this represents the first application of RL to this fundamental and widely used problem in computational algebra. The environment incorporates reward signals informed by domain expertise and is constructed to allow efficient estimation of the reward. We empirically validate the reward design by comparing it against measured runtimes, observing that it closely tracks computational complexity. We expect

that this reward formulation and environment design will be useful beyond the present work, supporting future research at the intersection of reinforcement learning and symbolic computation. We found that the scientific computing libraries in Python only allowed few fixed orderings; as a result we used Julia and wrote the RL environment from scratch. Our code and data are available [here](#).

Finally, we investigate whether the learned policies can be distilled into simpler, interpretable models. Using a synthetic dataset of over 100 problems, we train agents and attempt distillation into symbolic expressions and soft decision trees of varying complexity. These experiments suggest that the agents rely on a relatively small subset of exponent vectors when determining effective monomial orderings, indicating that careful subsampling may serve as a useful heuristic prior to optimization. At the same time, the distilled models fail to capture the full behavior of the learned policies. This provides empirical evidence that the agents exploit the subtle geometric structure of the Gröbner fan that is not easily represented by the basic interpretable models considered here. We outline potential directions for developing richer interpretable models in the concluding section.

1.2 Related work

The literature on Gröbner bases and its connections to algebraic geometry is extensive. Applications of Gröbner basis also form a vast literature. Rather than attempting a broad survey, we focus on prior work at the intersection of machine learning and Gröbner basis computation, which is most closely aligned with the aims of this paper.

A notable recent research direction, initiated by [34, 33], employs transformer models to predict Gröbner traces. While this line of work has shown promising results, it addresses a complementary problem. Our focus is not on predicting traces produced by a fixed algorithm, but on selecting monomial orderings that induce favorable traces for Buchberger’s algorithm. Other studies have applied machine learning to related symbolic computation tasks, including predicting the computational complexity of Gröbner basis computations [32] and optimizing elimination schemes in cylindrical algebraic decomposition [30, 29]. These works represent independent directions from our problem in this paper.

The work most closely related to ours is the ICML 2020 paper by Peifer, Stillman, and Halpern-Leistner [44], which applies reinforcement learning to optimize pair selection strategies in Buchberger’s algorithm. In their formulation, the learning environment changes substantially after each action, leading to a highly non-stationary setting that is computationally demanding and constrains large-scale experimentation. In contrast, we formulate monomial ordering selection as a stationary and comparatively simple reinforcement learning environment. This design choice is motivated by two considerations: reducing the computational cost of training and evaluation, and for preserving “clarity of direction” towards the goals of learning. The latter is inspired by recent evidence that relatively simple reinforcement learning schemes, such as Group Relative Policy Optimization (GRPO) [48], can be very effective when the underlying signal is well aligned with the task structure.

2 A Focused Introduction to Gröbner Bases and Buchberger's Algorithm

In this section, we briefly review key mathematical concepts and notation; for further details see [9]. Let k be a field and $R = k[x_1, \dots, x_n]$ the polynomial ring over k . Fix a monomial ordering \prec on R . For a nonzero polynomial $f \in R$, denote by $\text{LM}_\prec(f)$ and $\text{LT}_\prec(f)$ its leading monomial and leading term, respectively.

Definition 2.1. A finite set $G = \{g_1, \dots, g_t\} \subset I \subset R$ is a *Gröbner basis* of I with respect to \prec if

$$\langle \text{LT}_\prec(g_1), \dots, \text{LT}_\prec(g_t) \rangle = \langle \text{LT}_\prec(I) \rangle.$$

A Gröbner basis is *reduced* if each g_i is monic and no monomial of g_i is divisible by $\text{LM}_\prec(g_j)$ for $j \neq i$. For a fixed monomial order, every ideal admits a unique reduced Gröbner basis [9]. This does not imply, however, that every order will create a different reduced Gröbner basis as there are complex equivalences encoded by the Gröbner fan.

2.1 Monomial Orderings and Weight Vectors

A monomial ordering is a well-ordering on monomials that is compatible with multiplication. This means for every collection of monomials there will be a smallest one, and for any two monomials $x^\alpha = x_1^{\alpha_1} x_2^{\alpha_2} \cdots x_n^{\alpha_n}$ and $x^\beta = x_1^{\beta_1} \cdots x_n^{\beta_n}$ if x^α is ordered greater than x^β then $x^\alpha x^\gamma = x^{\alpha+\gamma}$ should be ordered greater than $x^\beta x^\gamma = x^{\beta+\gamma}$. These properties ensure we can perform division and elimination properly, and guarantee the termination of Gröbner basis algorithms. There is a convenient way to introduce monomial orders: Weight vectors $w = (w_1, \dots, w_n) \in \mathbb{R}_{>0}^n$ can be used to create orderings via

$$\deg_w(x^\alpha) = \sum_{i=1}^n w_i \alpha_i,$$

with ties broken by a secondary order. Allowing real weights is natural when studying Gröbner fans, since this ordering is invariant under multiplying all coordinates of the weight vector with a fixed scalar. We mentioned that most current implementations only allow a few fixed monomial orders derived from expert intuition. These orderings are

- **Lex:** Lexicographic ordering starting from x_1 to x_n (a limit of $w = (M^{n-1}, \dots, 1)$, $M \gg 1$),
- **GrLex:** This orders first with total degree and then breaks ties with lexicographic ordering (corresponding to $w = (1, \dots, 1)$).
- **GrevLex:** This orders first with total degree and then breaks ties with reverse-lexicographic ordering (corresponding to $w = (1, \dots, 1)$).

The choice of ordering strongly affects both the structure and the computational cost of the resulting Gröbner basis. There are theoretical and empirical results suggesting GrevLex is efficient, however, no general method exists for selecting an optimal order [9]: this is precisely the blind spot in conventional wisdom that this paper aims to clarify.

2.2 Buchberger's Algorithm and S-Polynomials

Buchberger's algorithm [5] is based on *S-polynomials*.

Definition 2.2. For nonzero $f, g \in R$,

$$S(f, g) = \frac{\text{lcm}(\text{LM}(f), \text{LM}(g))}{\text{LT}(f)} f - \frac{\text{lcm}(\text{LM}(f), \text{LM}(g))}{\text{LT}(g)} g.$$

A generating set G is a Gröbner basis if and only if all S-polynomials reduce to zero modulo G . Although conceptually simple, Buchberger's algorithm can exhibit severe intermediate expression growth and doubly exponential worst-case complexity [39]. For graded reverse lexicographic orderings, sharper single-exponential degree bounds are known [36, 16], motivating their widespread use.

2.3 The Gröbner Fan

For a fixed ideal $I \subset k[x_1, \dots, x_n]$, different monomial orders may yield distinct reduced Gröbner bases and initial ideals. The *Gröbner fan* [40, 23] provides a geometric framework for organizing this dependence using weight vectors $w \in \mathbb{R}^n$. For $f = \sum_{\alpha} c_{\alpha} x^{\alpha}$, the w -initial form $\text{in}_w(f)$ consists of terms with maximal $\langle w, \alpha \rangle$, and the associated initial ideal is

$$\text{in}_w(I) = \langle \text{in}_w(f) : f \in I \rangle.$$

As w varies, $\text{in}_w(I)$ remains constant on relatively open polyhedral cones and changes only when ties occur. These cones form a polyhedral fan whose full-dimensional cones are in bijection with the reduced Gröbner bases of I . Classical orders such as Lex, GrLex, and GrevLex correspond to specific directions or refinements within this fan. Figure 1 illustrates this structure schematically on a two-dimensional slice; it conveys how regions of constant initial ideal arise and how crossing a cone boundary corresponds to a combinatorial change in leading terms.

Example. Following Example 2.7 of [23], consider

$$I = \langle x + y + z, x^3 z + x + y^2 \rangle \subset \mathbb{Q}[x, y, z].$$

With lexicographic order $x \prec y \prec z$, a reduced Gröbner basis is

$$G_{\text{lex}}(I) = \{z + y + x, y^2 + x - x^3 y - x^4\},$$

so $\text{in}_{\text{lex}}(I) = \langle z, y^2 \rangle$. The corresponding Gröbner cone consists of weight vectors satisfying linear inequalities ensuring that these leading terms persist; when one of these inequalities becomes tight, the initial ideal changes.

2.4 The FGLM and F_4 Algorithms

For zero-dimensional ideals I , where R/I is finite-dimensional, the FGLM algorithm [19] converts a Gröbner basis under a degree-compatible order into one under another order

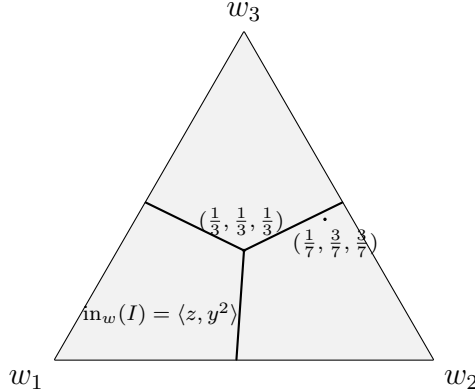


Figure 1: A schematic two-dimensional slice ($w_1 + w_2 + w_3 = 1, w \geq 0$) of the Gröbner fan for $I = \langle x + y + z, x^3z + x + y^2 \rangle$, illustrating how regions of constant $\text{in}_w(I)$ arise. The diagram is not to scale and is intended to convey the geometric structure of cones rather than exact fan boundaries; see [23].

using linear algebra. Modern variants are commonly used to transform from a fast monomial ordering to Lex, and the computation is effective in applications; see [20, 4].

Faugère’s F_4 algorithm [17] accelerates Buchberger’s method by batching reductions and performing them via structured linear algebra. At each stage, selected S-polynomials and multiples of basis elements are assembled into a matrix whose rows correspond to polynomials and columns to monomials. A subroutine of F_4 called symbolic preprocessing constructs this matrix, after which reduction is performed by Gaussian elimination. F_4 exploits the specific sparsity patterns of these matrices for high performance.

The dominant cost of F_4 is governed by the dimensions of these matrices. In particular, the number of columns, denoted by n_M in our reward formulation, captures the size of the active monomial basis and directly determines memory usage and linear algebra cost. Degree growth increases these dimensions and depends strongly on the monomial order. Since computation proceeds incrementally through such matrix constructions, these quantities provide natural proxies for computational effort and are used as feedback signals in our RL environment design.

3 Reinforcement Learning Setup

3.1 Problem Formulation and Environment Design

The problem we study is highly sensitive to changes in the support set (the collection of all exponent vectors present in the equations). In contrast, it exhibits significantly less sensitivity to variations in the coefficients of the defining equations, provided the monomials remain fixed. This observation was known from computer vision applications, where coefficients vary across problem instances while the support set remains constant; consequently, the trace Gröbner basis computation remains relatively stable. We leverage this stability in our environment design. The reinforcement learning environment consists of thousands of problem instances, and the reward is estimated by sampling these instances and computing the average reward.

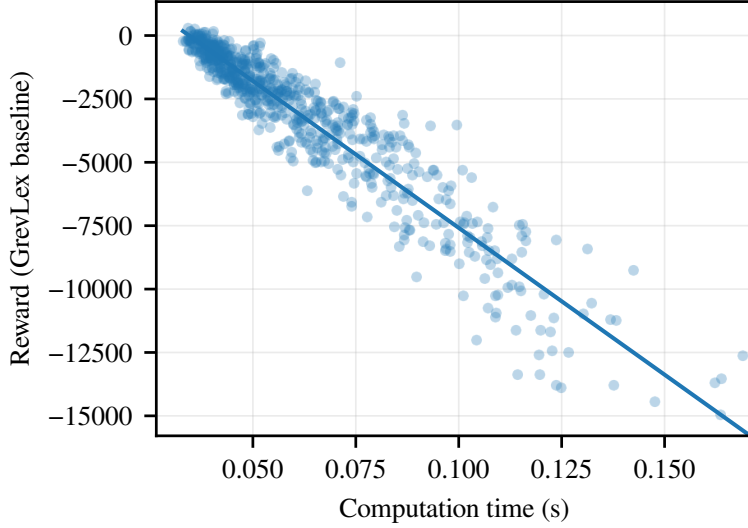


Figure 2: Reward improvement (relative to GrevLex) versus runtime for Gröbner basis computation on a fixed randomly generated ideal. Each point corresponds to a weighted monomial ordering with weights $(i, j, k) \in \{30, 35, \dots, 70\}^3$ ($N = 729$).

3.2 Computational Framework

Common Python-facing computational algebra tooling we considered does not expose the weighted monomial order search space and trace statistics we required. To address this, we utilized the Julia package `Groebner.jl` [13]. Our decision to use `Groebner.jl` was motivated primarily by its accessibility and efficiency.

1. **Accessibility:** It is highly approachable for researchers outside the computational algebra community.
2. **Efficiency:** It implements the F4 algorithm, which is an efficient yet relatively straightforward variant of Buchberger’s method.

Since the Julia reinforcement learning ecosystem is not as mature as Python’s, we developed our RL environment from scratch. Our code is available at the following repository.

3.3 Reward Function

Our reward function utilizes the Gröbner trace statistics of the F4 algorithm recorded by `Groebner.jl`, specifically: the number of iterations (t), the number of columns in the elimination matrix ($n_M(i)$) for $1 \leq i \leq t$, the number of pairs ($n_P(i)$), and the degree of pairs ($d_P(i)$). The reward function is defined as:

$$-\sum_{i=1}^t n_M(i)n_P(i) \ln(d_P(i))$$

The intuition behind this formulation is that the degree contributes to evaluation complexity on a logarithmic scale ($\ln(d)$), while the primary discrete parameters governing cost are the pair count and the size of the matrix.

We validated this reward by sweeping 729 weighted orderings on a fixed randomly generated ideal and comparing reward improvement over GrevLex against the measured runtime of computing a Gröbner Basis. The relationship is strongly monotone (Pearson $r = -0.949$, Spearman $\rho = -0.937$; see Figure 2). In our implementation we used the expert intuition, GrevLex, as a base-line for our rewards. This has two justifications: using a good baseline reduces the noise in training, and we have the easy interpretation that the agent is rewarded only when doing better than GrevLex and punished otherwise.

3.4 Action Space and Weight Vectors

The `Groebner.jl` package accepts only integer entries in weight vectors for the monomial ordering. However, the theoretical search space is the simplex:

$$\Delta_n := \{x = (x_1, x_2, \dots, x_n) : x_i \geq 0, \sum x_i = 1\}$$

Therefore, we define the action space as the simplex and define a monomial ordering by scaling the action vector by 10^3 and rounding to the nearest integer.

3.5 Agent Interaction and Training

At each step during an episode, the agent outputs a weight vector that defines a weighted monomial order. Using this order, we run a Gröbner basis computation and obtain a reward given by a Monte Carlo approximation of the reward using sample instances. The agent then updates the weight vector and repeats. An episode consists of a fixed number of such updates and terminates after L steps. We treat the episode length L and the number of training episodes N as hyper-parameters. Rewards are averaged over a batch of $B = 10$ ideals per step, where each ideal is instantiated from the same support set and uses uniform random coefficients from the finite field $\mathbb{F}_{32003} = \mathbb{Z}/32003\mathbb{Z}$. In experiments on ideals arising in systems biology and computer vision, we found $N = 10,000$ episodes and $L = 25$ steps per episode to work well.

An important practical detail is that a weight vector coordinate approaching zero effectively ignores a variable. This represents a degenerate choice from an algebraic perspective and introduces instability in practical computations. Consequently, we experimented with shrinking the action space by enforcing a lower bound on every coordinate, requiring $x_i \geq n^{-\alpha}$ for various integer values of α .

3.6 Model Architecture

Due to the sensitivity of the problem to input changes and our limited computational resources, we utilized the TD3 architecture with a prioritized replay buffer for its stability and efficiency [22, 47]. We experimented with various activation functions to address vanishing gradients including GELU (Gaussian Error Linear Unit) [28], but found that ReLU worked well in most cases. See Table 4 in Appendix A for the neural network architecture used in

Table 1: RL agent test performance (pooled over 5 seeds). Win, Tie, Loss mean percentages are reported along with mean percent reward improvement conditioned on wins and mean percent reward degradation conditioned on losses. Testing was done over 500,000 test ideals (100,000 per seed).

Polynomial System	GrevLex baseline			GrLex baseline		
	Win/Tie/Loss	Improvement	Degradation	Win/Tie/Loss	Improvement	Degradation
Relative Pose	98.4 / 0.0 / 1.6	19.43	-1.27	32.2 / 16.1 / 51.6	7.95	-7.04
Triangulation	27.0 / 66.1 / 7.0	0.86	-0.72	100 / 0 / 0	37.62	-
n -Site Phos. ($n=14$)	100 / 0 / 0	70.77	-	100 / 0 / 0	70.77	-
Wnt Shuttle	91.6 / 0.0 / 8.4	54.64	-26.40	86.9 / 0.0 / 13.1	55.25	-20.83

the experiments. Additionally, we tested different architectures with memory, such as an LSTM for the actor component of TD3, but observed only marginal performance improvements. We suspect this may be due to the current scale of our ideals, and further large-scale experimentation may provide deeper insights. Finally, needless to say that like most RL implementations, we performed extensive hyperparameter tuning to optimize the performance (see Appendix A).

4 Experiments on Problems from Systems Biology and Computer Vision

We tested the RL model on several important polynomial systems arising in computer vision, including minimal problems in relative pose with unknown focal length [49] and three-view triangulation [50], as well as models from systems biology such as the n -site phosphorylation system [24] and the Wnt shuttle model [26]. See Table 1 for the main results.

The RL models were all trained on Google Cloud Compute Engine instances. For the relative pose problem, three-view triangulation, and n -site phosphorylation ($n = 14$) we used a *c4-highcpu-8* instance (8 vCPUs, 16 GB Memory). For the Wnt shuttle model system we used a *c4-highmem-8* instance (8 vCPUs, 62 GB Memory) due to the size of the polynomial support set. See Appendix A for experimental details. The summary of results are presented in Table 1. We report the percentage of instances where the agents outperform standard heuristics during testing, the percentage of improvement in those cases, and the percentage of degradation when agents were beaten by expert heuristics. We should note that relative pose, triangulation, and n -site phosphorylation are polynomial systems in 3, 3, and 2 variables respectively, while the Wnt shuttle model yields a system in 19 variables. This is reflected in the RL training curves, with more variables leading to a larger search space and greater variance during training.

4.1 Relative Pose with Unknown Focal Length

This benchmark is the two-view relative pose problem where both cameras are calibrated up to a *shared unknown focal length* (with otherwise fixed intrinsics such as centered principal point, unit aspect ratio, and zero skew) [49]. Given six point correspondences (the minimal case), one estimates the epipolar geometry and the focal parameter by enforcing the epipolar

constraint together with the essential-matrix constraints induced by the unknown focal length [49]. The resulting constraints yield a polynomial system that can be expressed in the linear form $MX = 0$, where $M \in \mathbb{R}^{10 \times 33}$ and X is a vector of monomials in the chosen unknowns [49]. In our experiments we order the unknowns as (l_1, l_2, p) and use the associated monomial support listed in Appendix E.1.

After training, the RL agent was evaluated on 500,000 test ideals pooled over five random seeds. As shown in Table 1, the learned ordering substantially outperforms GrevLex on the relative pose system, winning in 98.4% of test instances with a mean reward improvement of 19.4% when it wins, and only rare degradations (1.6% losses with a mean degradation of 1.3%). In contrast, performance relative to GrLex is mixed, with the agent winning in 32.2% of cases and losing in 51.6%, reflecting the strong suitability of GrLex for this problem. These results indicate that the RL agent reliably discovers orderings competitive with or superior to standard heuristics, particularly compared to GrevLex. The final learned weight vectors across seeds are reported in Appendix B.1 (see Table 6).

4.2 Three-View Triangulation

Optimal three-view triangulation seeks a 3D point $X \in \mathbb{P}^3$ (homogeneous coordinates) minimizing the sum of squared reprojection errors in three calibrated views:

$$C(X) = \sum_{i=1}^3 d(P_i X, x_i)^2,$$

where $P_i \in \mathbb{R}^{3 \times 4}$ are known projection matrices and x_i are observed image points [50]. The stationary conditions $\partial C / \partial X_j = 0$ ($j = 1, 2, 3, 4$) can be cleared of denominators to obtain polynomial equations in the homogeneous coordinates [50]. Using the homogeneity of C , one reduces to three simultaneous degree-6 polynomial equations in the inhomogeneous variables (x, y, z) (after fixing scale by setting $t = 1$) [50]. We order variables as (x, y, z) and use the supports listed in Appendix E.2.

After training, the RL agent was evaluated on 500,000 test ideals pooled over five random seeds. As shown in Table 1, the learned ordering performs comparably to GrevLex on the three-view triangulation system, with a majority of test instances resulting in ties (66.1%) and only modest gains when the agent wins (mean improvement 0.86%). We should note that triangulation is seed-sensitive: one seed attains near-universal wins against GrevLex, while the remaining seeds are dominated by ties (Appendix B.2). In contrast, the agent consistently outperforms GrLex, winning on all test instances with a mean reward improvement of 37.6%. This pattern indicates that GrevLex already induces a near-optimal ordering for this problem, while the RL agent reliably avoids the substantial inefficiencies associated with GrLex. Overall, the learned ordering matches the strongest classical heuristic while remaining robust across baseline choices. The final learned variable weight vectors across seeds are located in Appendix B.2 (see Table 8).

4.3 n -Site Phosphorylation System

This benchmark comes from a sequential n -site phosphorylation/dephosphorylation mechanism modeled with mass-action kinetics and conservation laws [24]. For the class of subnet-

works considered in [24], the phosphatase total is constant, so substituting a (positive) monomial parametrization of steady states reduces the conservation relations to a system of *two* equations in the two unknowns (s_0, e) (unphosphorylated substrate and kinase) [24]. Equivalently, the reduced steady-state equations can be written in sparse matrix form $CX = 0$ with $C \in \mathbb{R}^{2 \times (n+3)}$ and X a vector of the $(n+3)$ monomials appearing in the two equations [24]. In our experiments we set $n = 14$ (so $|X| = 17$) and order variables as (s_0, e) , using the shared support listed in Appendix E.3.

After training, the RL agent was evaluated on 500,000 test ideals pooled over five random seeds. As shown in Table 1, the learned ordering consistently outperforms both GrevLex and GrLex on the n -site phosphorylation system, winning on all test instances against both baselines and achieving a large mean reward improvement of 70.8%. No degradations were observed in either comparison. These results indicate that the RL agent reliably discovers highly effective monomial orderings for this class of sparse biochemical systems, substantially improving upon standard heuristics. The final variable weight vectors across seeds can be found in Appendix B.3 (see Table 10).

4.4 Wnt Shuttle Model

The Wnt shuttle model captures protein shuttling between cellular compartments and the regulation and degradation of β -catenin within the Wnt signaling pathway [38]. Mathematically, it is formulated as a mass-action reaction network with 19 species (variables x_1, \dots, x_{19}) and 31 reaction-rate parameters k_1, \dots, k_{31} [26]. The dynamics admit five independent linear conservation relations, introducing conserved totals c_1, \dots, c_5 [26]. Steady states are characterized by the 19 polynomial equations $\dot{x}_i = 0$ together with the five conservation laws, yielding a polynomial system of 24 equations in the 19 species variables (with parameters appearing in coefficients) [26]. We use the monomial supports of these polynomials as listed in Appendix E.4 (see Equation (7)).

After training, the RL agent was evaluated on 500,000 test ideals pooled over five random seeds. As shown in Table 1, the learned ordering substantially outperforms both GrevLex and GrLex on the Wnt shuttle system, winning in 91.6% and 86.9% of test instances, respectively. When the agent improves upon the baseline, the gains are large, with mean reward improvements exceeding 54% in both comparisons. However, the agent also exhibits non-negligible losses relative to both heuristics, reflecting the complexity of this large polynomial system. These results demonstrate that the RL agent frequently identifies orderings that significantly accelerate Gröbner basis computation on the Wnt shuttle model, while occasional degradations remain. The final variable weight vectors across seeds are reported in Appendix B.4 (see Table 12).

5 Policy Distillation

To better understand the successful strategies of the agents, we generated a synthetic dataset comprising over 100 polynomial systems where the RL agents outperformed default heuristics (see Table 2). We attempted to distill these learned strategies into interpretable formats using two methods: soft decision trees and symbolic equations. Soft decision trees provide a trainable and interpretable model and has been used in policy distillation successfully, see

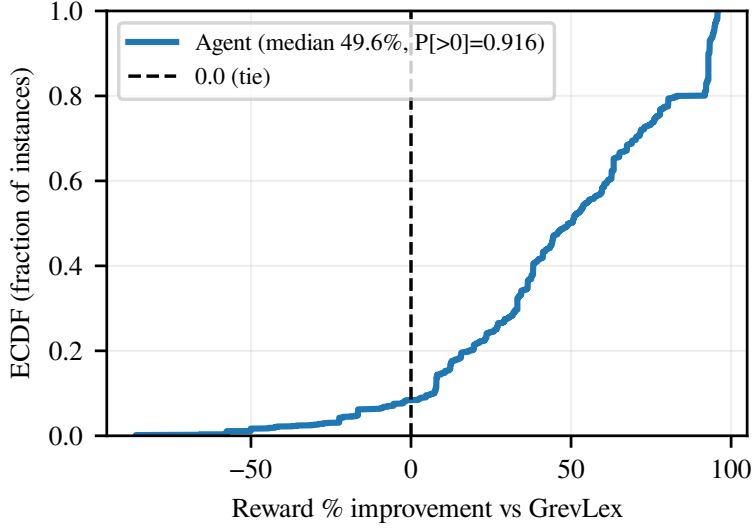


Figure 3: WNT shuttle model: empirical CDF of per-instance test-time reward percent improvement relative to GrevLex, $\Delta r\% = 100 (r_{\text{agent}} - r_{\text{GrevLex}}) / (|r_{\text{GrevLex}}| + \varepsilon)$ (pooled over 5 seeds; 10^5 test ideals per seed). The dashed vertical line marks $\Delta r\% = 0$ (tie); values to the right indicate instances where the agent achieves higher reward than GrevLex. The median improvement is 49.6% and $\Pr[\Delta r\% > 0] = 0.916$.

Table 2: Average RL agent reward performance against GrevLex and GrLex over synthetic ideals.

RL Agent vs Baseline	Win %	Improvement %
RL Agent vs GrLex	99.04	16.70
RL Agent vs GrevLex	94.78	11.70

[25]. Fitting symbolic equations is the canonical method in basic sciences and has seen a current surge of interest in interpretable machine learning in general and for policy distillation in particular [11, 37].

5.1 Symbolic Regression

We used `SymbolicRegression.jl` [10] to search for simple closed-form equations mapping polynomial ideal support sets to monomial ordering weight vectors. Following the default MLJ selection rule in `SymbolicRegression.jl`, we selected a single expression from the discovered Pareto frontier for each target as the highest-scoring expression among those with loss at most 1.5 times the minimum loss on the frontier (see Appendix C.1). We trained separate symbolic regression models to predict each entry of the weight vector (for $n = 3$ variables, this yields 3 equations). The selected equations were then fixed and evaluated by comparing the monomial order induced by the predicted variable weights against GrevLex.

5.2 Complexity of the Gröbner Fan

While the distilled decision trees achieved low Mean Squared Error (MSE) on training data, they exhibited limited generalization on previously unseen test sets. Similarly, the best-fit symbolic equations (detailed in Appendix C) displayed high variance in performance. They surpass expert heuristics on some ideals while failing on others.

Rather than a limitation of the training process, we interpret this result as empirical evidence of the intrinsic complexity of the problem. The optimal ordering is determined by the Gröbner fan, a complex structure where “wall-crossing” results in discrete jumps in computational cost. The inability of simple interpretable models to generalize suggests that the RL agents are successfully encoding high-dimensional, nonlinear geometric dependencies that defy compression into simple symbolic rules or shallow trees. This validates the necessity of deep reinforcement learning for this task, as the agent navigates a landscape too subtle for standard regression techniques.

5.3 The “Sparse Dependence” Heuristic

Despite the complexity of agent strategies, the distillation process revealed a structural insight. Both the decision trees (visualized in Appendix D) and symbolic expressions tended to rely on a small, specific subset of exponent vectors to make decisions. This indicates that the optimal ordering is often sensitive to a “critical set” of monomials rather than the entire support. This observation suggests a practical general heuristic for future work: performing careful subsampling of the support set and using this smaller group to decide on a monomial order.

In summary, while the agent’s strategy is irreducible to a simple formula, the distillation confirms that the agent exploits sparse dependencies within the polynomial support to navigate the complex geometry of the problem.

6 Discussion and Outlook

We have shown that reinforcement learning provides a flexible and effective framework for optimizing Gröbner basis computations, challenging the long-standing reliance on static defaults such as GrevLex. By formulating monomial ordering selection as a learned policy, our agents consistently outperform expert intuition across a range of polynomial systems arising in computer vision and systems biology reducing the cost metric up to 70%. Our work is the first result that uses machine learning (more specifically RL) on this widely applicable and important problem from computational algebra of selecting monomial orderings. We summarize our basic observations and promising future directions for improvement below.

Geometry of Learning. Our distillation experiments reveal a notable dichotomy. While reinforcement learning agents are able to navigate the optimization landscape effectively, the strategies they learn resist compression into simple symbolic rules or low-complexity decision models. This behavior suggests that the agents exploit the intricate, high-dimensional structure of the Gröbner fan, where effective decisions depend on subtle and nonlinear interactions among features of the polynomial support set.

These observations naturally point beyond the scope of the present study. In particular, they motivate future directions aimed at obtaining a generalizable model across families of problems and to design architectures that are interpretable by design for this particular problem.

Generalizable Models via Graph Neural Networks. The agents studied in this work are specialized to fixed polynomial support structures. A natural next step is to pursue more general-purpose neural Gröbner optimizers that can transfer across different supports. One promising direction is the use of Graph Neural Networks (GNNs), which can represent polynomial support sets as permutation-invariant graphs encoding relationships among monomials. Such architectures may enable learning policies that generalize beyond individual problem instances, reducing or eliminating the need for per-support training while preserving sensitivity to geometric structure.

Interpretable-by-Design Architectures. To narrow the gap between agent performance and human interpretability, future work should also explore interpretable-by-design learning architectures. Rather than producing unrestricted weight vectors, agents could be constrained to select from a structured vocabulary of parametrized geometric predicates. By forcing decisions to be expressed in terms of discrete geometric concepts, such models may yield strategies that are both effective and mathematically transparent, offering deeper insight into the geometry underlying efficient Gröbner basis computation.

Acknowledgments

We thank Tim Duff, Elias Tsigaridas, and Sameer Agarwal for helpful discussions. This work was carried out at the NSF REU Site in Mathematical Analysis and Applications at the University of Michigan–Dearborn. A.E. was partially supported by NSF-CCF-2414160 and by personal donations from Ketan Khowala, and all authors were partially supported by the National Science Foundation (DMS-2243808).

References

- [1] Sameer Agarwal, Timothy Duff, Max Lieblich, and Rekha R Thomas. An atlas for the pinhole camera. *Foundations of Computational Mathematics*, 24(1):227–277, 2024.
- [2] Félix Almendra-Hernández, Jesús A De Loera, and Sonja Petrović. Markov bases: a 25 year update. *Journal of the American Statistical Association*, 119(546):1671–1686, 2024.
- [3] Gregory Bard. *Algebraic cryptanalysis*. Springer Science & Business Media, 2009.
- [4] Jérémie Berthomieu, Vincent Neiger, and Mohab Safey El Din. Faster change of order algorithm for gröbner bases under shape and stability assumptions. In *Proceedings of the 2022 International Symposium on Symbolic and Algebraic Computation*, pages 409–418, 2022.

[5] Bruno Buchberger. *An Algorithm for Finding the Basis Elements of the Residue Class Ring of a Zero-Dimensional Polynomial Ideal*. PhD thesis, University of Innsbruck, 1965. English translation published in SIGSAM Bulletin, 2006.

[6] David A Cohen, Martin C Cooper, Páidí Creed, Peter G Jeavons, and Stanislav Zivny. An algebraic theory of complexity for discrete optimization. *SIAM Journal on Computing*, 42(5):1915–1939, 2013.

[7] Pasqualina Conti and Carlo Traverso. Buchberger algorithm and integer programming. In *International symposium on applied algebra, algebraic algorithms, and error-correcting codes*, pages 130–139. Springer, 1991.

[8] Nicolas Courtois, Alexander Klimov, Jacques Patarin, and Adi Shamir. Efficient algorithms for solving overdefined systems of multivariate polynomial equations. In *International Conference on the Theory and Applications of Cryptographic Techniques*, pages 392–407. Springer, 2000.

[9] David Cox, John Little, and Donal O’Shea. *Ideals, Varieties, and Algorithms*. Springer, 4 edition, 2015.

[10] Miles Cranmer. Interpretable machine learning for science with pysr and symbolic regression. jl. *arXiv preprint arXiv:2305.01582*, 2023.

[11] Miles Cranmer, Alvaro Sanchez Gonzalez, Peter Battaglia, Rui Xu, Kyle Cranmer, David Spergel, and Shirley Ho. Discovering symbolic models from deep learning with inductive biases. *Advances in neural information processing systems*, 33:17429–17442, 2020.

[12] Jesús A De Loera, Raymond Hemmecke, and Matthias Köppe. *Algebraic and geometric ideas in the theory of discrete optimization*. SIAM, 2012.

[13] Alexander Demin and Shashi Gowda. Groebner.jl: A package for gröbner bases computations in julia, 2024.

[14] Persi Diaconis and Bernd Sturmfels. Algebraic algorithms for sampling from conditional distributions. *The Annals of statistics*, 26(1):363–397, 1998.

[15] Alicia Dickenstein. Algebraic geometry tools in systems biology. *Notices of the American Mathematical Society*, 67, 2020.

[16] Thomas W. Dubé. The structure of polynomial ideals and gröbner bases. *SIAM Journal on Computing*, 19(4):750–773, 1990.

[17] Jean-Charles Faugère. A new efficient algorithm for computing gröbner bases (f_4). *Journal of Pure and Applied Algebra*, 139(1–3):61–88, 1999.

[18] Jean Charles Faugere. A new efficient algorithm for computing gröbner bases without reduction to zero (f 5). In *Proceedings of the 2002 international symposium on Symbolic and algebraic computation*, pages 75–83, 2002.

- [19] Jean-Charles Faugère, Patrizia Gianni, Daniel Lazard, and Teo Mora. Efficient computation of zero-dimensional gröbner bases by change of ordering. *Journal of Symbolic Computation*, 16(4):329–344, 1993.
- [20] Jean-Charles Faugère and Chenqi Mou. Sparse FGLM algorithms. *Journal of Symbolic Computation*, 80:538–569, 2017.
- [21] Martin Feinberg. *Foundations of chemical reaction network theory*. Springer, 2019.
- [22] Scott Fujimoto, Herke Hoof, and David Meger. Addressing function approximation error in actor-critic methods. In *International conference on machine learning*, pages 1587–1596. PMLR, 2018.
- [23] Komei Fukuda, Anders N. Jensen, and Rekha R. Thomas. Computing gröbner fans. *Mathematics of Computation*, 76(260):2189–2212, 2007.
- [24] Magalí Giaroli, Rick Rischter, Mercedes Pérez Millán, and Alicia Dickenstein. Parameter regions that give rise to $2\lfloor n/2 \rfloor + 1$ positive steady states in the n -site phosphorylation system. *arXiv preprint arXiv:1904.11633*, 2019.
- [25] Gargya Gokhale, Seyed Soroush Karimi Madahi, Bert Claessens, and Chris Develder. Distill2explain: Differentiable decision trees for explainable reinforcement learning in energy application controllers. In *Proceedings of the 15th ACM International Conference on Future and Sustainable Energy Systems*, pages 55–64, 2024.
- [26] Elizabeth Gross, Heather A. Harrington, Zvi Rosen, and Bernd Sturmfels. Algebraic systems biology: A case study for the wnt pathway. *Bulletin of Mathematical Biology*, 78:21 – 51, 2016.
- [27] Richard Hartley and Andrew Zisserman. *Multiple view geometry in computer vision*. Cambridge university press, 2004.
- [28] Dan Hendrycks and Kevin Gimpel. Gaussian error linear units (gelus). *arXiv preprint arXiv:1606.08415*, 2016.
- [29] Zongyan Huang, Matthew England, James H Davenport, and Lawrence C Paulson. Using machine learning to decide when to precondition cylindrical algebraic decomposition with groebner bases. In *2016 18th International Symposium on Symbolic and Numeric Algorithms for Scientific Computing (SYNASC)*, pages 45–52. IEEE, 2016.
- [30] Zongyan Huang, Matthew England, David Wilson, James H Davenport, Lawrence C Paulson, and James Bridge. Applying machine learning to the problem of choosing a heuristic to select the variable ordering for cylindrical algebraic decomposition. In *International Conference on Intelligent Computer Mathematics*, pages 92–107. Springer, 2014.
- [31] Mike Innes. Flux: Elegant machine learning with julia. *Journal of Open Source Software*, 2018.

- [32] Shahrzad Jamshidi, Eric Kang, and Sonja Petrović. Predicting the cardinality and maximum degree of a reduced gröbner basis. *arXiv preprint arXiv:2302.05364*, 2023.
- [33] Yuta Kambe, Yota Maeda, and Tristan Vaccon. Geometric generality of transformer-based gröbner basis computation. *arXiv preprint arXiv:2504.12465*, 2025.
- [34] Hiroshi Kera, Yuki Ishihara, Yuta Kambe, Tristan Vaccon, and Kazuhiro Yokoyama. Learning to compute gröbner bases. *Advances in Neural Information Processing Systems*, 37:33141–33187, 2024.
- [35] Viktor Larsson, Magnus Oskarsson, Kalle Aström, Alge Wallis, Zuzana Kukelova, and Tomas Pajdla. Beyond gröbner bases: Basis selection for minimal solvers. In *Proceedings of the IEEE Conference on Computer Vision and Pattern Recognition (CVPR)*, pages 3945–3954. IEEE, 2018.
- [36] Daniel Lazard. Gröbner bases, gaussian elimination and resolution of systems of algebraic equations. In *Proceedings of the European Computer Algebra Conference on Computer Algebra*, pages 146–156, 1983.
- [37] Peilang Li, Umer Siddique, and Yongcan Cao. Symbolic policy distillation for interpretable reinforcement learning. In *Mechanistic Interpretability Workshop at NeurIPS 2025*, 2025.
- [38] Adam L. MacLean, Zvi Rosen, Helen M. Byrne, and Heather A. Harrington. Parameter-free methods distinguish wnt pathway models and guide design of experiments. *Proceedings of the National Academy of Sciences*, 112(9):2652–2657, 2015.
- [39] Ernst W Mayr and Albert R Meyer. The complexity of the word problems for commutative semigroups and polynomial ideals. *Advances in mathematics*, 46(3):305–329, 1982.
- [40] Ferdinando Mora and Lorenzo Robbiano. The gröbner fan of an ideal. *Journal of Symbolic Computation*, 6(2–3):183–208, 1988.
- [41] James Nielsen and Bernard Roth. On the kinematic analysis of robotic mechanisms. *The International Journal of Robotics Research*, 18(12):1147–1160, 1999.
- [42] David Nistér. An efficient solution to the five-point relative pose problem. *IEEE transactions on pattern analysis and machine intelligence*, 26(6):756–770, 2004.
- [43] Aesun Park, Kyung-Ah Shim, Namhun Koo, and Dong-Guk Han. Side-channel attacks on post-quantum signature schemes based on multivariate quadratic equations: Rainbow and UOV. *IACR Transactions on Cryptographic Hardware and Embedded Systems*, pages 500–523, 2018.
- [44] Dylan Peifer, Michael Stillman, and Daniel Halpern-Leistner. Learning selection strategies in buchberger’s algorithm. In *International Conference on Machine Learning*, pages 7575–7585. PMLR, 2020.

- [45] Mercedes Pérez Millán and Alicia Dickenstein. The structure of messi biological systems. *SIAM Journal on Applied Dynamical Systems*, 17(2):1650–1682, 2018.
- [46] M Raghavan and B Roth. Solving polynomial systems for the kinematic analysis and synthesis of mechanisms and robot manipulators. *Journal of Mechanical Design*, 117(B):71–79, 1995.
- [47] Tom Schaul, John Quan, Ioannis Antonoglou, and David Silver. Prioritized experience replay. *arXiv preprint arXiv:1511.05952*, 2015.
- [48] Zhihong Shao, Peiyi Wang, Qihao Zhu, Runxin Xu, Junxiao Song, Xiao Bi, Haowei Zhang, Mingchuan Zhang, YK Li, Yang Wu, et al. Deepseekmath: Pushing the limits of mathematical reasoning in open language models. *arXiv preprint arXiv:2402.03300*, 2024.
- [49] Henrik Stewénius, David Nistér, Fredrik Kahl, and Frederik Schaffalitzky. A minimal solution for relative pose with unknown focal length. *Image and Vision Computing*, 26(7):871–877, 2008.
- [50] Henrik Stewénius, Frederik Schaffalitzky, and David Nistér. How hard is 3-view triangulation really? In *Proceedings of the Tenth IEEE International Conference on Computer Vision (ICCV'05)*, volume 1, pages 686–693. IEEE, 2005.
- [51] Seth Sullivant. *Algebraic Statistics*. American Mathematical Society, 2018.
- [52] Charles W Wampler and Andrew J Sommese. Numerical algebraic geometry and algebraic kinematics. *Acta Numerica*, 20:469–567, 2011.

A Experimental Details

Table 3: Hyper-parameter choices for the TD3 algorithm and PER buffer.

Algorithm	Hyper-parameter	Value
TD3	Training Episodes	10,000
	γ (Reward Discount Factor)	0.99
	τ (Target Network Update Rate)	0.05
	Initial Actor Learning Rate	10^{-4}
	Minimum Actor Learning Rate	10^{-5}
	Initial Critic Learning Rate	10^{-4}
	Minimum Critic Learning Rate	10^{-6}
	σ (Exploration Noise Std.)	0.002
	d (Policy Update Delay)	100
PER	Replay Buffer Capacity	1,000,000
	Sampling Batch Size	100
	α (Prioritization Exponent)	0.6
	β (Importance-Sampling Exponent)	0.4
	η (Beta Annealing Step Size)	10^{-4}
	ϵ (Priority Offset)	0.01

Setup and compute. We run all experiments with five random seeds per problem instance. The agents were all trained on Google Cloud Compute Engine instances. For the relative pose with unknown focal length problem, three-view triangulation, and n -site phosphorylation ($n = 14$) we used a *c4-highcpu-8* instance (8 vCPUs, 16 GB Memory). For the Wnt shuttle model system we used a *c4-highmem-8* instance (8 vCPUs, 62 GB Memory) due to the size of the polynomial support set. We utilized the Twin-Delayed Deep Deterministic Policy Gradient (TD3) algorithm alongside a prioritized experience replay (PER) buffer for the RL agent [22, 47].

Training procedure. During training, at each timestep, the actor outputs a real-valued weight vector $w \in \mathbb{R}^n$ (via a softmax), to which we add Gaussian exploration noise; the resulting vector is then discretized into integer weights by scaling by 10^3 , rounding to the nearest integer, and clamping each entry to be at least 1:

$$\tilde{w} = \max(\text{round}(10^3 \cdot w), 1),$$

where the $\max(\cdot, 1)$ is applied element-wise. We then pair \tilde{w} with the corresponding variables to construct a weighted monomial ordering. Using this order, we run Gröbner basis computation and obtain a reward given by a Monte Carlo approximation of the reward using sample instances. The agent then updates the weight vector and repeats. An episode consists of a fixed number of these updates and terminates after $L = 25$ steps, and we train for $N = 10,000$ episodes. Rewards are averaged over a batch of $B = 10$ ideals per step, where each ideal is instantiated from a fixed polynomial support set and uses uniform random coefficients from the finite field $\mathbb{F}_{32003} = \mathbb{Z}/32003\mathbb{Z}$.

Table 4: Neural network architectures used in TD3. We denote the flattened observation dimension by d_o .

Network	Architecture
Actor $\pi_\phi(o)$	Fully Connected: $d_o \rightarrow 512 \rightarrow 512 \rightarrow 512 \rightarrow n$, ReLU activations, Softmax output.
Critic $Q_\theta(o, a)$ (each of two)	Fully Connected: $(d_o + n) \rightarrow 512 \rightarrow 512 \rightarrow 512 \rightarrow 1$, ReLU activations.

State and action representation. The environment state $s_t \in \mathbb{R}^n$ is the current continuous variable weight vector. At the start of each episode, we initialize s_0 by sampling $\epsilon_i = 1 + u_i$ with $u_i \sim \text{Unif}(0, 1)$ independently and setting $s_0 = \epsilon / \|\epsilon\|_1$. The actor observes a fixed encoding of the polynomial support (the normalized monomial-exponent matrix for the base set) with s_t appended as an additional feature and flattened; the action a_t is a proposed next weight vector (actor output plus exploration noise), and the next state is set to $s_{t+1} = a_t$.

Optimization schedule. Both actor and critic learning rates are linearly decayed from their initial values to their minimum values over the first 90% of training episodes, and are held constant at the minimum for the remaining 10% of episodes. These initial and minimum learning rates are recorded in Table 3.

Evaluation protocol. We evaluate the trained policy without further learning. We first draw a *calibration batch* of $B = 100$ randomly generated ideals. For each ideal, we run the actor in the environment for 25 steps (which matches training) and record the final predicted weight vector, yielding a set of candidate orders. We score each of these candidates by applying it to the entire calibration batch and measuring the mean reward which involves computing Gröbner bases for the batch under that fixed order. We select the single best-performing order on this calibration batch. After selecting the final order, we generate a fresh test set of 100,000 new ideals *per seed* and report performance of the selected order on this set. The calibration and test ideals are generated independently using separate RNG seeds. Given the large coefficient field and the number of independently sampled coefficients per ideal, the collision probability is negligible.

Network architecture. We use an actor π_ϕ and two critics $Q_{\theta_1}, Q_{\theta_2}$ with corresponding target networks as in TD3. Both actor and critics are feed-forward neural networks with three linear hidden layers of width 512 and ReLU activation functions (Table 4). The actor maps the flattened observation vector (support-set features with the current weight state appended) to a length- n weight vector and applies a softmax. During training, we add Gaussian exploration noise to the actor output prior to discretization. Each critic takes as input the concatenation of the flattened observation and the action vector and outputs a scalar Q -value.

Initialization and reproducibility. Actor and critic networks were implemented in `Flux.jl` [31]. We used Flux’s default parameter initialization (`glorot_uniform` for linear layers). Target networks were initialized by copying the online networks prior to soft updates in TD3. We fix random seeds for coefficient sampling, dataset generation, and network initialization/training. Gröbner basis computations are performed using `Groebner.jl`, which may exhibit run-to-run nondeterminism despite seeding.

B Additional Results

In this section we present more detailed results from our experiments involving important ideals arising in computer vision and systems biology.

B.1 Relative Pose with Unknown Focal Length

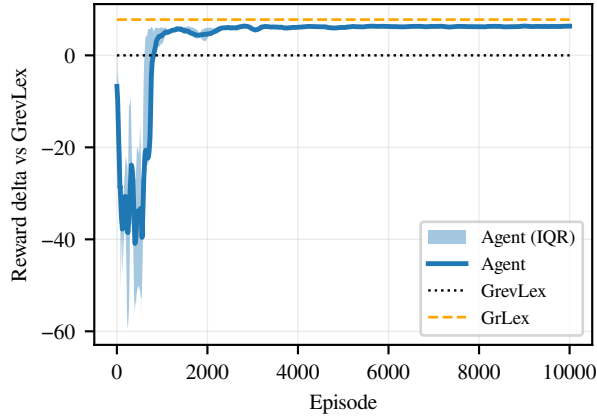


Figure 4: Mean agent reward for relative pose with unknown focal length system per training episode alongside GrevLex and GrLex baselines. Interquartile range (IQR) over seeds is shown in light blue.

Table 5: Relative Pose: reward robustness across seeds. Entries are median [IQR] across 5 seeds (10^5 test ideals per seed). For each seed we compute win/tie/loss rates and the per-seed mean percent change conditional on wins (improvement) or losses (degradation).

Metric	Agent vs GrevLex	Agent vs GrLex
Win rate (%)	98.546 [98.134, 98.551]	30.993 [28.462, 38.759]
Tie rate (%)	0.000 [0.000, 0.000]	0.000 [0.000, 37.664]
Loss rate (%)	1.454 [1.449, 1.866]	60.574 [31.343, 61.241]
Per-seed mean improvement on wins (%)	19.292 [19.280, 19.728]	8.191 [7.531, 8.428]
Per-seed mean degradation on losses (%)	-1.411 [-1.444, -0.957]	-7.366 [-10.028, -7.284]

Table 6: Final discretized agent weight vectors for the Relative Pose with Unknown Focal Length system across five random seeds. We report the integer weight vector $\tilde{w} = \max(\text{round}(10^3 \cdot w), 1)$ used to define the monomial order and the implied variable priority order. Bold indicates the seed with the largest estimated mean reward improvement vs. GrevLex, computed as $\hat{\Delta} = (\text{win}/100) \cdot (\text{improve_win_only}) + (\text{loss}/100) \cdot (\text{degrade_loss_only})$ (ties contribute 0).

Seed	Final discretized weights \tilde{w}	Implied variable order
0	(373, 305, 323)	$x_1 > x_3 > x_2$
1	(322, 297, 382)	$x_3 > x_1 > x_2$
2	(308, 313, 379)	$x_3 > x_2 > x_1$
3	(326, 352, 322)	$x_2 > x_1 > x_3$
4	(318, 373, 309)	$x_2 > x_1 > x_3$

B.2 Three-View Triangulation

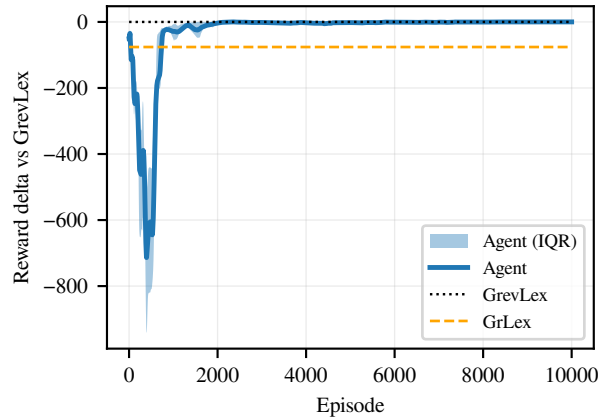


Figure 5: Mean agent reward for three-view triangulation system per training episode alongside GrevLex and GrLex baselines. Interquartile range (IQR) over seeds is shown in light blue.

Table 7: Triangulation: reward robustness across seeds. Entries are median [IQR] across 5 seeds (10^5 test ideals per seed). For each seed we compute win/tie/loss rates and the per-seed mean percent change conditional on wins (improvement) or losses (degradation).

Metric	Agent vs GrevLex	Agent vs GrLex
Win rate (%)	8.565 [8.486, 9.343]	100.000 [100.000, 100.000]
Tie rate (%)	82.822 [81.176, 83.136]	0.000 [0.000, 0.000]
Loss rate (%)	8.378 [8.322, 8.613]	0.000 [0.000, 0.000]
Per-seed mean improvement on wins (%)	0.715 [0.715, 0.716]	37.509 [37.508, 37.510]
Per-seed mean degradation on losses (%)	-0.724 [-0.724, -0.721]	—

Table 8: Final discretized agent weight vectors for the Three-View Triangulation system across five random seeds. We report the integer weight vector $\tilde{w} = \max(\text{round}(10^3 w), 1)$ used to define the monomial order and the implied variable priority order. Bold indicates the seed with the largest estimated mean reward improvement vs. GrevLex, computed as $\hat{\Delta} = (\text{win}/100) \cdot (\text{improve_win_only}) + (\text{loss}/100) \cdot (\text{degrade_loss_only})$ (ties contribute 0).

Seed	Final discretized weights \tilde{w}	Implied variable order
0	(230, 401, 369)	$x_2 > x_3 > x_1$
1	(311, 348, 340)	$x_2 > x_3 > x_1$
2	(371, 372, 257)	$x_2 > x_1 > x_3$
3	(264, 365, 371)	$x_3 > x_2 > x_1$
4	(355, 305, 340)	$x_1 > x_3 > x_2$

B.3 n -Site Phosphorylation System

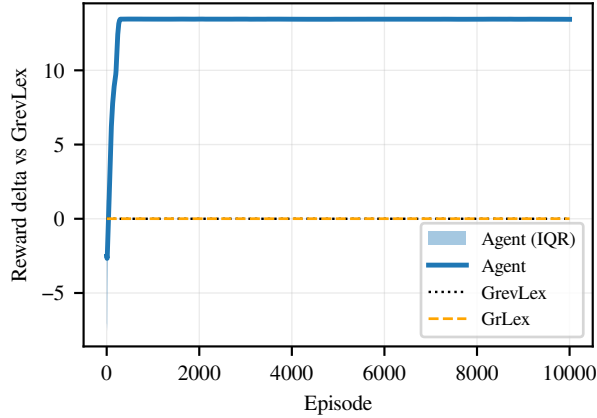


Figure 6: Mean agent reward for n -site phosphorylation system per training episode alongside GrevLex and GrLex baselines. Interquartile range (IQR) over seeds is shown in light blue.

Table 9: N-site phosphorylation: reward robustness across seeds. Entries are median [IQR] across 5 seeds (10^5 test ideals per seed). For each seed we compute win/tie/loss rates and the per-seed mean percent change conditional on wins (improvement) or losses (degradation).

Metric	Agent vs GrevLex	Agent vs GrLex
Win rate (%)	100.000 [100.000, 100.000]	100.000 [100.000, 100.000]
Tie rate (%)	0.000 [0.000, 0.000]	0.000 [0.000, 0.000]
Loss rate (%)	0.000 [0.000, 0.000]	0.000 [0.000, 0.000]
Per-seed mean improvement on wins (%)	70.770 [70.770, 70.771]	70.770 [70.769, 70.771]
Per-seed mean degradation on losses (%)	—	—

Table 10: Final discretized agent weight vectors for the n -Site Phosphorylation system across five random seeds. We report the integer weight vector $\tilde{w} = \max(\text{round}(10^3 w), 1)$ used to define the monomial order and the implied variable priority order. Bold indicates the seed with the largest estimated mean reward improvement vs. GrevLex, computed as $\hat{\Delta} = (\text{win}/100) \cdot (\text{improve_win_only}) + (\text{loss}/100) \cdot (\text{degrade_loss_only})$ (ties contribute 0).

Seed	Final discretized weights \tilde{w}	Implied variable order
0	(1000, 1)	$x_1 > x_2$
1	(1000, 1)	$x_1 > x_2$
2	(1000, 1)	$x_1 > x_2$
3	(955, 45)	$x_1 > x_2$
4	(983, 17)	$x_1 > x_2$

B.4 Wnt Shuttle Model

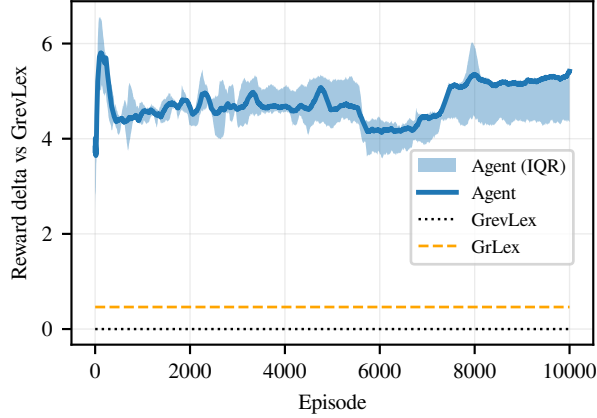


Figure 7: Mean agent reward for Wnt shuttle model system per training episode alongside GrevLex and GrLex baselines. Interquartile range (IQR) over seeds is shown in light blue.

Table 11: WNT: reward robustness across seeds. Entries are median [IQR] across 5 seeds (10^5 test ideals per seed). For each seed we compute win/tie/loss rates and the per-seed mean percent change conditional on wins (improvement) or losses (degradation).

Metric	Agent vs GrevLex	Agent vs GrLex
Win rate (%)	99.850 [99.212, 100.000]	96.475 [96.252, 100.000]
Tie rate (%)	0.000 [0.000, 0.000]	0.000 [0.000, 0.000]
Loss rate (%)	0.150 [0.000, 0.788]	3.525 [0.000, 3.748]
Per-seed mean improvement on wins (%)	39.319 [37.646, 69.656]	38.010 [35.288, 68.035]
Per-seed mean degradation on losses (%)	-8.274 [-17.562, -7.442]	-3.786 [-13.418, -3.079]

Table 12: Final discretized agent weight vectors for the Wnt Shuttle Model system across five random seeds. We report the integer weight vector $\tilde{w} = \max(\text{round}(10^3 w), 1)$ (only non-unit entries shown for readability; omitted entries equal 1) and the implied variable priority order. Bold indicates the seed with the largest estimated mean reward improvement vs. GrevLex, computed as $\widehat{\Delta} = (\text{win}/100) \cdot (\text{improve_win_only}) + (\text{loss}/100) \cdot (\text{degrade_loss_only})$ (ties contribute 0).

Seed	Final discretized weights \tilde{w} (sparse; non-ones)	Implied variable order
0	$x_{19}:1000$ (others 1)	$x_{19} > \text{others}$ (tied)
1	$x_{17}:1000$ (others 1)	$x_{17} > \text{others}$ (tied)
2	$x_2:512, x_5:434, x_{17}:11, x_3:10, x_{12}:9, x_7:6, x_{18}:6, x_{14}:5, x_{10}:2$ (others 1)	$x_2 > x_5 > x_{17} > x_3 > x_{12} > (x_7 = x_{18}) > x_{14} > x_{10} > \text{others}$
3	$x_2:1000$ (others 1)	$x_2 > \text{others}$ (tied)
4	$x_{16}:494, x_{17}:394, x_{13}:79, x_5:21, x_2:5, x_{19}:4, x_7:2$ (others 1)	$x_{16} > x_{17} > x_{13} > x_5 > x_2 > x_{19} > x_7 > \text{others}$

C Symbolic Regression Equations

C.1 Best Symbolic Regression Equations

$$w_1(x) = \frac{0.005620111648365623 x_{15}}{0.41764189247505734 - (x_{42} - x_{21})x_1} + 0.3285121764974553 \quad (1)$$

(see Table 13, Complexity 13)

$$w_2(x) = -0.002235617301013779 \left[\frac{x_{40} - (x_8 - x_{43})}{x_{29}x_{33} + 0.23181594905978833} \right. \\ \left. - \left(x_{33}x_9 + x_{29} \frac{-2.6092572238752862 x_{31}}{x_{24} + 0.8938154468830032} - (x_{51}x_{46} + x_{47}x_{37}) \right) \right] + 0.3591951413920924 \quad (2)$$

(see Table 14, Complexity 37)

$$w_3(x) = 0.0025153236949469683 \left[(x_{35} - (x_{45} - x_{18})) \left(x_{43} - 0.1117044718447674 x_{24}x_{15}x_{10} \right) + (x_{46} - x_{22})x_{47} \right. \\ \left. + \left(x_{45} - \left((x_{51} - (x_{46} - 2.472476686808669) - x_{21}) 0.4030994964706104 \right) - x_{15} \right)^2 \right] + 0.3125372513473696 \quad (3)$$

(see Table 15, Complexity 40)

C.2 Symbolic Regression Runner-ups

The following tables report the Hall of Fame expressions obtained through `SymbolicRegression.jl`. For each target, expressions are shown from the Pareto frontier, where complexity is measured by node count with each operator, variable, and constant contributing unit cost, and loss corresponds to mean squared error (L2DistLoss). Expressions are ordered by increasing complexity, and for each complexity level the expression with the lowest mean squared error is reported.

Table 13: Best equations at each complexity for x_1 weight.

Complexity	Loss	Equation
1	0.00084203	0.335353908454586
5	0.00080188	$-0.0046158769662659116 x_{33} + 0.34548194929346504$
6	0.00080159	$(- 0.0022266810459186485 x_{33} + 0.8085746701887174)^5$

7	0.00076023	$0.007101505925913343/(0.5008673141532315 - x_1) + 0.33771927404824137$
8	0.00075939	$0.006882074640602726/(0.39837595753768223 - x_1^4) + 0.33472540695934044$
9	0.00070293	$x_{15} 0.00031468880927016735/(0.02391101342623325 - x_1) + 0.33117132434738383$
10	0.00065630	$-0.007372465610914996/(x_3 - (x_1 + 0.5591087934678365)^3) + 0.3340533898078061$
12	0.00062627	$x_{15} 0.0015838879526246991/(x_3 - (x_1 - 0.4366839685254661)^3) + 0.3330674836798489$
13	0.00056414	$0.005620111648365623 x_{15}/(0.41764189247505734 - (x_{42} - x_{21})x_1) + 0.3285121764974553$
14	0.00055918	$0.0017032708532298386 x_{15}^2/(0.42069267319326054 - (x_{42} - x_{21})x_1) + 0.3301019930946452$
15	0.00054388	$0.00797284069124181 (x_{15} - 0.8129971943825058)/(0.4487955698570075 - (x_{42} - x_{21})x_1) + 0.33110916450723943$
16	0.00051155	$-0.001985966203118873 (x_3 - x_{15}^2)/(0.405649388473595 - (x_{42} - x_{21})x_1) + 0.3316337474494216$
17	0.00049757	$(x_{15} - 0.45311719799127026 x_3) (0.007098223286061685/(0.40730076571579676 - (x_{42} - x_{21})x_1)) + 0.3308134115589299$
18	0.00049701	$(0.0034905131345707146 (x_{15} - 0.4618026758965021 x_3)/(0.4312939940164463 - (x_{42} - x_{21})x_1) + 0.8015132923036502)^5$
19	0.00048087	$0.006779004173437662 (x_{15} - 0.24535182897116273 x_{11}x_3)/(0.4353455212996979 - (x_{42} - x_{21})x_1) + 0.3309002658196576$
20	0.00047959	$(- 0.5752651687819168 - 0.005957292217184054 (x_{15} - 0.25527858194238934 x_{11}x_3)/(0.4500364214761212 - (x_{42} - x_{21})x_1))^2$
21	0.00046960	$-0.013717485498834751 x_{15}/((x_{32}((x_{25} - 0.4069727000080694 x_{34})x_3)) - (0.8404253408504924 - x_1x_7)) + 0.3339296560732781$
22	0.00046185	$(- 0.5745563514052511 - 0.0054471371796765 (x_{15} + 0.3239162142722927(x_{17} - x_{11}x_3))/(0.47631273534124813 - (x_{42} - x_{21})x_1))^2$
23	0.00045559	$x_{15} (-0.014214964317353139/(x_1x_7 + x_{32}((x_{25} - 0.40063961198015563 x_{34})x_3) - 0.9081076188299587) + 0.002607236858603949) + 0.32883104309502337$
24	0.00044210	$(- 0.5755104167273538 - 0.006397558424129668 (x_{15} + 0.3203210787099133((x_{11} - x_{43})x_{11}x_3))/(0.4769463584228517 - (x_{42} - x_{21})x_1))^2$
26	0.00044192	$((x_{15} + 0.3097648286613735((x_{11} - x_{11}x_3) - (x_{43} + 0.24942426276230753)))(0.0065583064541704225/(0.47852394857981884 - (x_{42} - x_{21})x_1)) + 0.575664307607853)^2$

27	0.00043258	$(-0.014657285921587318/(x_7x_1 + x_{32}((x_2 - x_7 - 0.3960833348371273x_{34})(x_3 - 0.04753016637230385)) - 0.9318601830011407) + 0.0027135047221870136)x_{15} + 0.3279745155651019$
28	0.00042895	$(-0.5743323359043249 - (x_{15} + 0.3115162090541634((x_{11} - x_{11}x_3) - ((x_{43} + 1.8546631396767344) - x_{22})))^2(0.006476643266282883/(0.4822291194014101 - (x_{42} - x_{21})x_1)))^2$

Table 14: Best equations at each complexity for x_2 weight.

Complexity	Loss	Equation
1	0.00078947	0.333991507716237
5	0.00075544	$-0.004199115704102301x_{46} + 0.3425935796304692$
6	0.00075529	$(-0.0020277713924658834x_{46} + 0.8071924178529383)^5$
7	0.00072033	$-0.0021130167799510383x_{47}x_{31} + 0.3403100433298779$
8	0.00071989	$(0.8061166767001957 - 0.0010366330129766433x_{31}x_{47})^5$
9	0.00066067	$0.0010987382178416394x_{31}x_{46}x_{47} + 0.34090395786341393$
10	0.00065699	$-0.0003371555036407168x_{47}x_{31}x_{46}^2 + 0.34008649358858045$
11	0.00062943	$0.0020338646068404674x_{31}(x_{19} - x_{46} - x_{47}) + 0.3407644743185726$
13	0.00060744	$0.0021405969477780082(x_{45} + x_{31}(x_{19} - x_{46} - x_{47})) + 0.3363607121050117$
15	0.00058262	$0.0025081350655382258(x_{45} + x_{31}(x_9 - x_{46} - x_{47}) + x_{33}) + 0.33097200530614007$
17	0.00055884	$0.00191878170741938((x_{31}x_{46} - x_{45})/(-0.3060438988542676 - x_{24}) - x_{37}x_{47}) + 0.3451167234987364$
19	0.00051931	$(x_{46}x_{51} - 0.0022148380626643926(x_{37} - (x_{33} + x_{31}/(-0.44420884210847517 - x_{24}))x_{39})) + 0.3490547776658768$
20	0.00051481	$(x_{51}x_{46} - 0.0023200756665093906(x_{37} - (x_{31}/(-0.781593885421935 - x_{24})^3 + x_{33})x_{39})) + 0.3471331687446784$
21	0.00048898	$0.00236733598928659(((x_{31}/(-0.456255437752778 - x_{24}) + x_{33}) - x_{37})x_{39} - (x_{50} + x_{46}x_{51})) + 0.3551263876805231$
22	0.00048675	$0.002443052189456914(x_{39}((x_{33} - x_{37}) + x_{31}/(-0.7859361386370655 - x_{24})^3) - (x_{51}x_{46} + x_{50})) + 0.35308082825021847$

Table 14: Best equations at each complexity for x_2 weight.

Complexity	Loss	Equation
23	0.00046503	$0.0018248037128027186 \left(\left((x_{31}/(-0.38099333741954855 - x_{24}) + x_{33} - x_{50})x_{39} \right) - (x_{47}x_{37} + x_{51}x_{46}) \right) + 0.35378347325409515$
24	0.00046297	$\left(-0.5949846470208265 - 0.001586193251114419(x_{39}(x_{33} + x_{31}/(-0.37200420537481116 - x_{24}) - x_{50}) - (x_{51}x_{46} + x_{47}x_{37})) \right)^2$
25	0.00044263	$\left(x_{46}x_{51} - 0.001914639887438814((x_{37} - (x_8 - x_2))x_{47} - x_{39}(x_{31}/(-0.382712551548299 - x_{24}) + x_{33})) \right) + 0.3473789455394515$
26	0.00044159	$\left(-0.5893700679989564 + 0.0016580897566988162((x_{47}(x_{37} - (x_8 - x_2)) + x_{46}x_{51}) - x_{39}(x_{31}/(-0.373203831216098 - x_{24}) + x_{33})) \right)^2$
27	0.00042545	$\left((x_{47}(x_{37} - (x_8 - x_2)) + x_{51}x_{46}) - (x_{33} + (x_{31}/(-0.3321670393695553 - x_{24}) - x_{12}))x_{39} \right) (-0.0018145013437147934) + 0.35446315781549986$
29	0.00041140	$\left(((x_{37} - (x_8 - x_{41}))x_{47}) - (x_{23} + (x_{33} + x_{31}/(-0.33046765097746766 - x_{24}) - x_{12})x_{39}) + x_{46}x_{51} \right) (-0.0018098846467069424) + 0.35019788451166994$
31	0.00041134	$\left(((x_{37} - (x_8 - x_{41}))x_{47}) - (x_{23} + (x_{33} + x_{31}/(-0.33046765097746766 - x_{24}) - (x_{12} - 0.17452676144906673))x_{39}) + x_{46}x_{51} \right) (-0.0018098846467069424) + 0.35019788451166994$
32	0.00040966	$\left(x_{43}/(x_{29}^3 + 0.21668132336426366) - ((x_{33}x_9) + x_{29}((x_{31}/(x_{24} + 0.9799775476388732))(-3.1441422538653527)) - (x_{46}x_{51} + x_{24}x_{47})) \right) (-0.002171787760626936) + 0.35919383963827073$
33	0.00038691	$0.0021205150448707823 \left(((x_{31}x_{29})/(x_{24} + 0.8466651252176755))(-2.614565853580865) - (x_{51}x_{46} + x_{47}x_{37}) + x_9x_{33} - x_{40}/(x_{29}x_{33} + 0.19545647402663877) \right) + 0.3594572066076611$
35	0.00035425	$0.002244557052296696 \left(x_9x_{33} - (x_{51}x_{46} + x_{47}x_{37}) + ((x_{29}x_{31})(-2.5146823106334244))/(x_{24} + 0.8636999456811458) - (x_{40} - (x_8 - x_{43}))/(x_{29} + 0.22228327081320715) \right) + 0.35955925873265626$

Table 14: Best equations at each complexity for x_2 weight.

Complexity	Loss	Equation
36	0.00035230	$0.002272116513640928 \left(\left(\left(-2.6090149778032843/(x_{24} + 0.8973959852574365) \right) x_{29} \right) x_{31} - (x_{47}x_{37} + x_{46}x_{51}) + x_{33}x_9 - (x_{40} - (x_8 - x_{43}))/(x_{29}^2 + 0.2264743324062024) \right) + 0.3592286936836383$
37	0.00033215	$-0.002235617301013779 \left(\left(x_{40} - (x_8 - x_{43}) \right)/(x_{29}x_{33} + 0.23181594905978833) - (x_{33}x_9 + (x_{29}((x_{31}(-2.6092572238752862))/(x_{24} + 0.8938154468830032)) - (x_{51}x_{46} + x_{47}x_{37}))) \right) + 0.3591951413920924$
38	0.00033147	$0.002244425401757337 \left(\left(x_{29}x_{31}(-2.6093339340107944)/(x_{24} + 0.8945511162213898) + (x_9x_{33} - (x_{46}x_{51} + x_{47}x_{37})) - (x_{40} - (x_8 - x_{43}))/(x_{33}x_{29}^2 + 0.2339784392837013) \right) + 0.35891790936256646$
40	0.00033098	$\left((x_{51}x_{46} + x_{37}x_{47}) - ((x_{45} - x_{53}) - (x_{40} - (x_8 - x_{43}))/(x_{29}^4 + 0.2417138822628581) + x_{33}x_9 + (x_{29}x_{31}(-2.7453391278876245))/(x_{24} + 0.9560107774969062)) \right) (-0.00230981887182462) + 0.3588645590624389$
41	0.00032537	$0.0021996038348656905 \left(x_{33}(x_9 + 0.9992791933740277) + x_{31}(x_{29}(-2.829653528461395/(x_{24} + 0.9326840103556284))) - (x_{37}x_{47} + x_{51}x_{46}) + x_{45} - (x_{40} - (x_8 - x_{43}))/(x_{29} + 0.22762105258676915) - x_{53} \right) + 0.3545816332666742$
42	0.00032388	$0.002233692909954876 \left((x_9 + 0.9192291261504111)x_{33} + (x_{29}(x_{31}(-2.8589974979019375/(x_{24} + 0.9481617496027702))) - (x_{37}x_{47} + x_{51}x_{46}) + x_{45} - x_{53}) - (x_{40} - (x_8 - x_{43}))/(x_{29}^2 + 0.23352143425750302) \right) + 0.35450471133492284$
43	0.00031733	$0.002338160881345756 \left(((x_{31}(-2.8152793987412856) - x_{43}(-0.7773759055994179))x_{29})/(x_{24} + 0.8522483091384043) + (x_{45} - x_{53}) - (x_{47}x_{37} + x_{46}x_{51}) + x_{33}x_9 - (x_{40} - (x_8 - x_{43}))/(x_{29} + 0.2500061705458608) \right) + 0.35790957885390356$
45	0.00030834	$0.0023014495193051394 \left(x_{45} - (x_{40} - (x_8 - x_{43}))/(x_{29} + 0.2447808603451855) + (x_9 + 0.8456580509874632)x_{33} - (x_{51}x_{46} + x_{47}x_{37}) + ((x_{31}(-2.827475727728687) - x_{43}(-0.7779616422592833))x_{29})/(x_{24} + 0.819637925080654) - x_{53} \right) + 0.3537012271375328$

Table 14: Best equations at each complexity for x_2 weight.

Complexity	Loss	Equation
47	0.00030677	$0.0023273398597252405 \left(x_{45} + (x_9 + 0.7608004910166554)x_{33} - (x_{47}x_{37} + x_{51}x_{46}) - x_{53} + ((x_{31}(-2.8319135217202875) - x_{43}(-0.7538195202526867))x_{29})/(x_{24} + 0.82042160941259) - ((x_{40} + 0.5594128253067995) - (x_8 - x_{43}))/x_{29} + 0.27076459337861525 \right) + 0.3554408433301304$
49	0.00030674	$0.9115388333286707 \left(0.002544728786040382 \left(x_{45} + (x_9 + 0.7653057555117491)x_{33} - (x_{51}x_{46} + x_{37}x_{47}) - x_{53} + (x_{29}(x_{31}(-2.834934086133134) - x_{43}(-0.7514412054558395)))/(x_{24} + 0.821887430914458) - ((x_{40} + (0.5595340556515455 - (x_8 - x_{43}))/x_{29} + 0.2715583381850336) \right) + 0.3897378324018952 \right)$

 Table 15: Best equations at each complexity for x_3 weight.

Complexity	Loss	Equation
1	0.00087608	0.33065458382200147
5	0.00082794	$0.0049947168548858814 x_{46} + 0.320422688130653$
6	0.00082254	$8.042901951560854 \times 10^{-5} x_{43}^4 + 0.3254954135905829$
7	0.00078902	$0.004545560610712497 (x_{46} + x_{43}) + 0.31256060469366886$
8	0.00075318	$0.3366298173974247 - 1.0092803392911087 \times 10^{-5} x_{15} x_{21}^5$
9	0.00073919	$0.33131528802674354 - 0.0021952429973046412 x_{15} (x_{21} - x_{51})$
10	0.00069402	$0.33157528202583064 + 4.5834661596589784 \times 10^{-5} x_{15}^4 (x_{51} - x_{21})$
11	0.00065058	$0.3325734057882249 - 0.004033442088750746 (x_{51} - x_{21})(x_1 - x_{15})$
12	0.00063675	$8.56259399681715 \times 10^{-5} x_5 (x_{51} - x_{21}) x_{15}^3 + 0.3324602104413529$
13	0.00059392	$0.3312978884974693 + 0.002175888564310824 x_5 (x_{51} - x_{21}) (x_{15} - 1.6545830265253603)$
14	0.00058819	$0.3321442926473853 + 0.0010229333922801703 (x_{15}^2 - x_1 x_{45})(x_{51} - x_{21})$
15	0.00055270	$0.33833886120375295 + 0.002129155628770091 x_5 ((x_{51} - x_{21})(x_{15} - 1.8194694713075403) - x_{11})$
16	0.00055264	$(0.5815316989581872 + 0.0018580403870196221 x_5 ((x_{51} - x_{21})(x_{15} - 1.8063902347770566) - x_{11}))^2$
17	0.00049840	$0.33044428516462354 + 0.0022218664448306253 x_5 (((x_{15} - 1.9345985168978028)(x_{51} - x_{21}) + x_{43}) - x_{11})$
19	0.00047904	$0.3355111863721219 - 0.0023188669021414637 (x_5(x_{11} - (x_{43} + (x_{51} - x_{21})(x_{15} - 1.9273556047791913))) + x_{39})$

Table 15: Best equations at each complexity for x_3 weight.

Complexity	Loss	Equation
21	0.00046841	$0.33842817649545387 - 0.0022827681332977198(x_5(x_{11} - (x_{43} - (x_{51} - x_{21})(x_{15} - 1.9897227444584367))) + x_{39}x_8)$
23	0.00046485	$-0.0022684016080321712(x_{22} - x_5((x_{51} - x_{21})(x_{15} - 1.8943375090532004) + x_{43} - 0.3957861122866493x_{12}x_{11})) + 0.3327055940376386$
25	0.00045836	$0.3331880635541003 + 0.002229994470279145x_5((x_{15} - 1.9168858125859567)(x_{51} - x_{21}) - 0.36987256794841716x_{12}x_{11} + x_{43} - x_{44}/1.7948234686692892)$
26	0.00045676	$0.3352609855215257 + 0.000968590126591488((x_{12} - 0.6265352014847679)x_{26}(x_{46} - x_{11} - x_8) + (x_{51} - x_{21})(x_{15}^2 - x_{45}x_1))$
27	0.00044707	$0.33148505384565896 + 0.0025266111034353417x_5(-0.3125198732383364x_{11}x_{12} + (x_{51} - x_{21})(x_{15} - 1.9064262470349407) + x_{43} - x_{26}/(x_9 + 1.1262315507580507))$
28	0.00044220	$0.002816834926431939((x_{35} - (x_{45} - x_{18}))(x_{43} - 0.26704001906409974x_{15}x_{10}) + x_{47}(x_{46} - x_{22}) + (x_{45} - x_{15})^2) + 0.3136529125025496$
29	0.00043477	$0.33148250482799 + 0.002432353906894396x_5(-0.30819736508643114x_{12}x_{11} + x_{43} + (x_{51} - x_{21})(x_{15} - 1.9237359137999686) - x_{26}/(x_9x_{46} + 1.1512804582845528))$
30	0.00038809	$0.002743153299578441((x_{35} - (x_{45} - x_{18}))(x_{43} - 0.10659040733797036x_{24}x_{10}x_{15}) + x_{47}(x_{46} - x_{22}) + (x_{15} - x_{45})^2) + 0.3138307221906743$
32	0.00037873	$0.0028183583126295706((x_{35} - (x_{45} - x_{18}))(x_{43} - 0.11116423563988116x_{24}x_{15}x_{10}) + (x_{46} - x_{22})x_{47} + x_{24} + (x_{15} - x_{45})^2) + 0.30741446558876223$
34	0.00036038	$0.0023427157748366328(((x_{45} - (x_{51} - x_{21}))0.7292014270107886 - x_{15})^2) + x_{45}(x_{46} - x_{22}) + ((x_{35} - (x_{45} - x_{18}))(x_{43} - 0.28395945551346546x_{10}x_{15})) + 0.31289431057379996$

Table 15: Best equations at each complexity for x_3 weight.

Complexity	Loss	Equation
36	0.00033513	$0.0025656042317600243 \left(x_{47}(x_{46} - x_{22}) + ((x_{15} - (x_{45} - 0.3808200991158191(x_{51} - x_{21})))^2 + (x_{35} - (x_{45} - x_{18}))(x_{43} - 0.10286795355494745 x_{15}x_{10}x_{24})) \right) + 0.3123325801690137$
38	0.00032179	$0.0023279484917965547 \left(x_{10} + ((0.7053528913176984(x_{45} - (x_{51} - x_{21})) - x_{15})^2) + x_{47}(x_{46} - x_{22}) + (x_{35} - (x_{45} - x_{18}))(x_{43} - 0.12042537845498498 x_{15}x_{24}x_{10}) \right) + 0.30903266715539784$
40	0.00029808	$0.0025153236949469683 \left((x_{35} - (x_{45} - x_{18}))(x_{43} - 0.1117044718447674 x_{24}x_{15}x_{10}) + (x_{46} - x_{22})x_{47} + (x_{45} - 0.4030994964706104(x_{51} - x_{46} - 2.472476686808669 - x_{21}) - x_{15})^2 \right) + 0.3125372513473696$
42	0.00029334	$0.002559798232109027 \left((x_{35} - (x_{45} - x_{18}))(x_{43} - 0.10673373507090549 x_{10}x_{24}x_{15}) + (x_{45} - 0.33261097044161836(x_{51} - x_{46} + x_7 - x_{21}) - x_{15})^2 + x_{47}(x_{46} - x_{22}) + x_{51} \right) + 0.306355949551514$
44	0.00027908	$0.002490439657321843 \left((x_{46} - x_{22})x_{47} + (x_{35} - (x_{45} - x_{18}))(x_{43} - 0.12624988881508498 x_{15}x_{24}x_{10}) + (x_{45} - 0.4440134981610858(x_{51} - 0.5187357361284024(x_{46} - x_{23} - x_7) - x_{21}) - x_{15})^2 \right) + 0.31244325316937577$
46	0.00026917	$0.0024897226018737156 \left(x_{10} + (x_{15} - (x_{45} - 0.47724653358206776(x_{51} - 0.4999848079129539(x_{46} - x_{23} - x_7) - x_{21}))^2 + (x_{35} - (x_{45} - x_{18}))(x_{43} - 0.1344127470430672 x_{15}x_{24}x_{10}) + (x_{46} - x_{22})x_{47} \right) + 0.30744355777844795$
48	0.00025901	$0.0025884970138480242 \left((x_{46} - x_{22})x_{47} + (x_{45} - 0.455787070592263(x_{51} - 0.4805310670016915(x_{46} - x_{23} - x_7) - x_{21}) - x_{15})^2 + (x_{35} - (x_{45} - x_{18}))(x_{43} - 0.1367129133385923 x_{24}x_{10}x_{15}) + (x_{10} + x_{24}) \right) + 0.3013569751203911$
50	0.00025835	$0.0025958429222822923 \left(((x_{46} - x_{22}) + 0.34991507947644734 x_{10})x_{47} + (x_{35} - (x_{45} - x_{18}))(x_{43} - 0.13643454842977537 x_{10}x_{24}x_{15}) + x_{24} + (x_{15} - (x_{45} - 0.4396520838509348(x_{51} - 0.4892197777096199(x_{46} - x_{23} - x_7) - x_{21})))^2 \right) + 0.3031685893578367$

D Decision Tree Illustrations

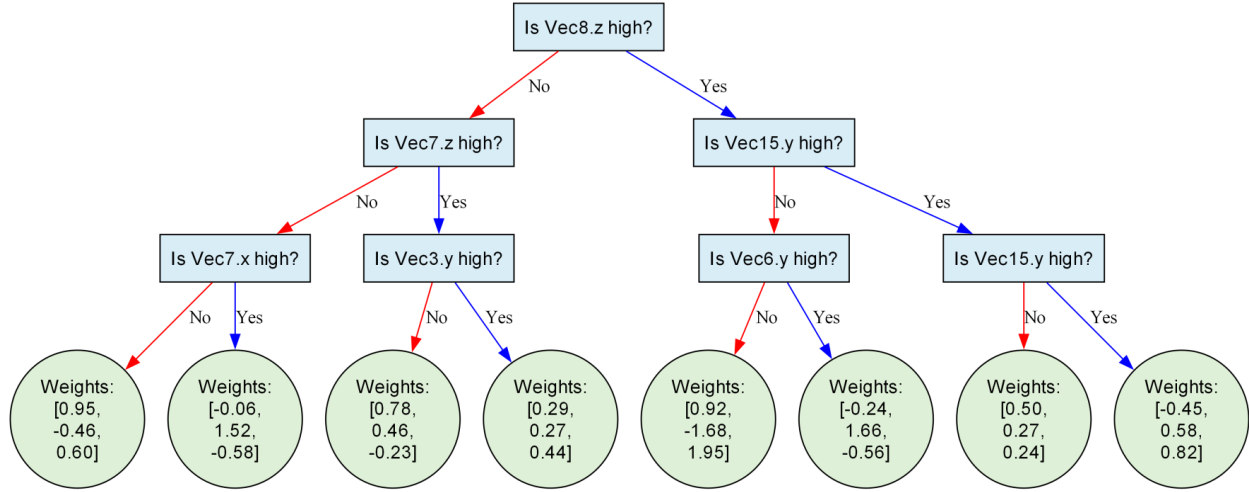


Figure 8: Depth 3 soft-decision tree

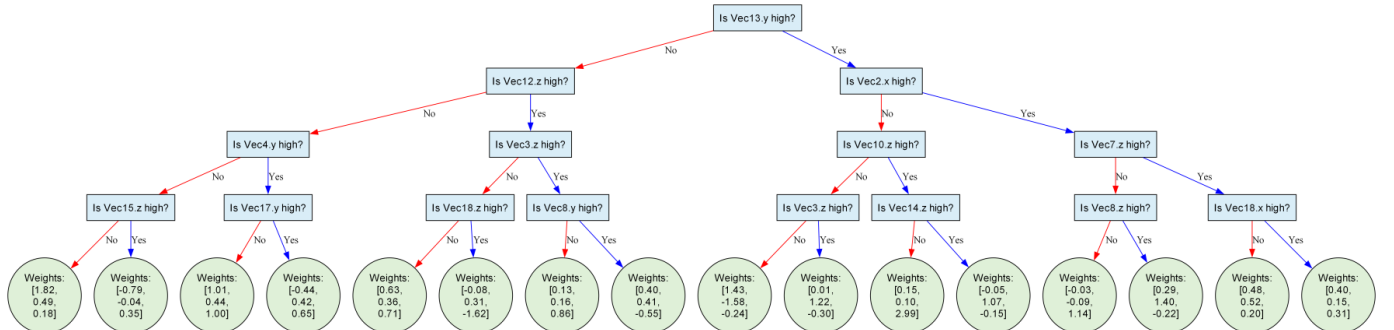


Figure 9: Depth 4 soft-decision tree



Figure 10: Depth 6 soft-decision tree

E Polynomial Support Sets for Experiments

E.1 Relative pose with unknown focal length

Ordering variables as (l_1, l_2, p) , the ten polynomials have support set (i.e. the exponent vectors of the monomials in X):

$$\mathcal{A} = \left\{ (3, 0, 2), (3, 0, 1), (3, 0, 0), (2, 1, 2), (1, 2, 2), (0, 3, 2), (2, 1, 1), (1, 2, 1), (0, 3, 1), (2, 1, 0), (1, 1, 2), (2, 0, 2), (0, 2, 2), (1, 0, 3), (1, 2, 0), (0, 3, 0), (2, 0, 1), (0, 1, 3), (1, 1, 1), (0, 2, 1), (1, 0, 2), (0, 1, 2), (0, 0, 3), (2, 0, 0), (1, 1, 0), (0, 2, 0), (1, 0, 1), (0, 1, 1), (0, 0, 2), (1, 0, 0), (0, 1, 0), (0, 0, 1), (0, 0, 0) \right\}. \quad (4)$$

E.2 Three-view triangulation

Ordering variables as (x, y, z) , the three polynomials have support sets:

$$\begin{aligned} \mathcal{A}_1 &= \left\{ (4, 2, 0), (4, 0, 2), (3, 3, 0), (3, 2, 1), (3, 2, 0), (3, 1, 2), (3, 0, 3), (3, 0, 2), (1, 3, 2), (1, 2, 3), (1, 2, 2), (0, 4, 2), (0, 3, 3), (0, 3, 2), (0, 2, 4), (0, 2, 3), (0, 2, 2) \right\}, \\ \mathcal{A}_2 &= \left\{ (4, 0, 2), (3, 3, 0), (3, 1, 2), (3, 0, 3), (3, 0, 2), (2, 4, 0), (2, 3, 1), (2, 3, 0), (2, 1, 3), (2, 1, 2), (2, 0, 4), (2, 0, 3), (2, 0, 2), (1, 3, 2), (0, 4, 2), (0, 3, 3), (0, 3, 2) \right\}, \\ \mathcal{A}_3 &= \left\{ (4, 2, 0), (3, 3, 0), (3, 2, 1), (3, 2, 0), (3, 0, 3), (2, 4, 0), (2, 3, 1), (2, 3, 0), (2, 2, 1), (2, 2, 0), (2, 1, 3), (2, 0, 4), (2, 0, 3), (1, 2, 3), (0, 3, 3), (0, 2, 4), (0, 2, 3) \right\}. \end{aligned} \quad (5)$$

E.3 n -site phosphorylation system ($n = 14$)

Ordering variables as (s_0, e) , both polynomials share the same support set:

$$\mathcal{A} = \left\{ (1, 0), (0, 1), (1, 1), (1, 2), (1, 3), (1, 4), (1, 5), (1, 6), (1, 7), (1, 8), (1, 9), (1, 10), (1, 11), (1, 12), (1, 13), (1, 14), (0, 0) \right\}. \quad (6)$$

E.4 Wnt shuttle model system

Ordering variables as $(x_1, x_2, \dots, x_{19})$, the twenty-four polynomials have support sets:

$$\begin{aligned}
\mathcal{A}_1 &= \left\{ (1, 0) \right\}, \\
\mathcal{A}_2 &= \left\{ (1, 0), (0, 1, 0), \right. \\
&\quad (0, 0, 1, 0), (0, 1, 0), \\
&\quad \left. (0, 0, 0, 0, 0, 0, 0, 0, 0, 0, 0, 0, 0, 0, 0, 1, 0, 0, 0, 0, 0, 0) \right\}, \\
\mathcal{A}_3 &= \left\{ (0, 1, 0, 0, 0, 0, 0, 0, 0, 0, 0, 0, 0, 0, 0, 0, 0, 0, 0, 0, 0), (0, 0, 1, 0, 0, 0, 0, 0, 0, 0, 0, 0, 0, 0, 0, 0, 0, 0, 0, 0, 0, 0), \right. \\
&\quad (0, 0, 1, 0, 0, 1, 0, 0, 0, 0, 0, 0, 0, 0, 0, 0, 0, 0, 0, 0, 0, 0, 0, 0), (0, 0, 0, 0, 0, 0, 0, 0, 0, 0, 0, 0, 0, 0, 0, 0, 0, 0, 0, 1, 0, 0, 0, 0, 0), \\
&\quad \left. (0, 0, 1, 0, 1, 0, 0, 0, 0, 0, 0, 0, 0, 0, 0, 0, 0, 0, 0, 0, 0, 0, 0) \right\}, \\
\mathcal{A}_4 &= \left\{ (0, 1, 0, 1, 0, 0, 0, 0, 0, 0, 0, 0, 0, 0, 0, 0, 0, 0, 0, 0, 0, 0), (0, 0, 0, 1, 0, 0, 0, 0, 0, 0, 0, 0, 0, 0, 0, 0, 0, 0, 0, 0, 0, 0), \right. \\
&\quad (0, 0, 0, 0, 0, 0, 0, 0, 0, 0, 0, 0, 0, 0, 0, 1, 0, 0, 0, 0, 0, 0), (0, 1, 0, 0, 0), \\
&\quad \left. (0, 1, 0) \right\}, \\
\mathcal{A}_5 &= \left\{ (0, 0, 0, 0, 1, 0, 0, 0, 0, 0, 0, 0, 0, 0, 0, 0, 0, 0, 0, 0, 0, 0), (0, 0, 0, 0, 0, 0, 1, 0, 0, 0, 0, 0, 0, 0, 0, 0, 0, 0, 0, 0, 0, 0), \right. \\
&\quad (0, 0, 0, 0, 1, 0, 0, 1, 0, 0, 0, 0, 0, 0, 0, 0, 0, 0, 0, 0, 0, 0), (0, 0, 0, 0, 0, 0, 0, 0, 0, 0, 0, 0, 0, 0, 0, 0, 0, 0, 0, 1, 0, 0, 0, 0, 0), \\
&\quad \left. (0, 1, 0, 0, 0) \right\}, \\
\mathcal{A}_6 &= \left\{ (0, 0, 1, 0, 0, 1, 0, 0, 0, 0, 0, 0, 0, 0, 0, 0, 0, 0, 0, 0, 0, 0), (0, 0, 0, 0, 0, 1, 0, 0, 0, 0, 0, 0, 0, 0, 0, 0, 0, 0, 0, 0, 0, 0), \right. \\
&\quad (0, 0, 0, 0, 0, 0, 0, 0, 0, 0, 0, 0, 0, 0, 0, 1, 0, 0, 0, 0, 0), (0, 1, 0, 0), \\
&\quad \left. (0, 1) \right\}, \\
\mathcal{A}_7 &= \left\{ (0, 0, 0, 0, 1, 0, 0, 0, 0, 0, 0, 0, 0, 0, 0, 0, 0, 0, 0, 0, 0, 0), (0, 0, 0, 0, 0, 0, 1, 0, 0, 0, 0, 0, 0, 0, 0, 0, 0, 0, 0, 0, 0, 0), \right. \\
&\quad (0, 0, 0, 0, 0, 0, 1, 0, 0, 0, 0, 0, 0, 0, 0, 0, 0, 0, 0, 0, 0, 0), (0, 1, 0, 0, 0), \\
&\quad \left. (0, 1, 0, 0) \right\}, \\
\mathcal{A}_8 &= \left\{ (0, 0, 0, 0, 1, 0, 0, 1, 0, 0, 0, 0, 0, 0, 0, 0, 0, 0, 0, 0, 0, 0) \right\}, \\
\mathcal{A}_9 &= \left\{ (0, 0, 0, 0, 0, 1, 0, 1, 0, 0, 0, 0, 0, 0, 0, 0, 0, 0, 0, 0, 0, 0, 1, 0, 0) \right\}, \\
\mathcal{A}_{10} &= \left\{ (0, 0), (0, 0), \right. \\
&\quad (0, 0, 0, 1, 0, 0, 0, 0, 0, 1, 0, 0, 0, 0, 0, 0, 0, 0, 0, 0, 0, 0), (0, 0, 0, 0, 0, 0, 0, 0, 0, 0, 0, 0, 0, 0, 0, 0, 0, 0, 0, 1, 0, 0, 0, 0), \\
&\quad \left. (0, 1, 0, 0) \right\}, \tag{7}
\end{aligned}$$

